arXiv:1404.5091v2 [cond-mat.mtrl-sci] 5 May 2014

Re-t_{2g}-splitting-driven semiconductor gaps in ferrimagnetic double perovskite Ca_2MReO_6 (M=Cr,Fe) from first-principles

Sai Gong, San-Dong Guo, Peng Chen and Bang-Gui Liu*
Beijing National Laboratory for Condensed Matter Physics, Institute of Physics, Chinese Academy of Sciences, Beijing 100190, China
(Dated: May 6, 2014)

Motivated by the observation of nonmetallic nature in double perovskite Ca_2CrReO_6 and Ca_2FeReO_6 with high magnetic Curie temperatures of 360 and 522 K, we systematically investigate the structural, electronic, and magnetic properties of Ca_2MReO_6 (M=Cr,Fe) using the full-potential linear augmented plane wave (FP-LAPW) method within the density functional theory. Our full optimization confirms the stable ground-state structure with $P2_1/n$ symmetry. The modified Becke-Johnson (mBJ) exchange potential is used for investigating electronic structures. Our mBJ calculation shows that they are both ferrimagnetic semiconductors with semiconductor gaps of 0.38 eV and 0.05 eV, respectively, in contrast with wrong metallic phases from the generalized gradient approximation (GGA). The origin of semiconductor gap is due to the further distortion of ReO_6 octahedra caused by John-Teller effect, which drives the three partially-occupied Re t_{2g} bands split into two fully-filled bands and one empty band in the minority-spin channel. With the spin-orbit coupling (SOC) taken into account, the Ca_2MReO_6 (M=Cr,Fe) shows high magneto-crystalline anisotropy (MCA) with the magnetic easy axis along pseudocubic [010] direction, and the total magnetic moments increase by $0.209\mu_B$ and $0.258\mu_B$ per formula unit, respectively, due to the strong SOC effect on Re ion. Although reducing to 0.31 and 0.03 eV, the semiconductor gaps remain open in spite of the SOC broadening of the Re t_{2g}-related bands. Therefore, our DFT investigation with mBJ has established the correct ferrimagnetic semiconductor ground state for the double perovskites Ca_2MReO_6 (M=Cr,Fe). This mechanism, different from that in double perovskite Sr_2CrOsO_6, can help understand physical properties of other similar compounds.

PACS numbers: 75.30.-m,75.50.-y,75.10.-b,71.20.-b

I. INTRODUCTION

Because of their rich physics and high technological potential[1], ordered double perovskite $A_2BB'O_6$ (A = alkali, alkaline-earth or rare-earth ion; B and B' = transition metals) have been extensively studied[2–18]. For cubic or tetragonal double perovskite $Sr_2BB'O_6$ (B = Cr or Fe, and B' = Mo, W, or Re), ferrimagnetic metallic phase is usually formed because the fully occupied high spin state Fe^{3+} ($3d^5$) or Cr^{3+} ($3d^3$) is antiferromagnetically coupled with the partially filled $4d$ and $5d$ transition-metal cations[18,19]. Among them, half-metallic Sr_2FeMoO_6, Sr_2FeReO_6, and Sr_2CrReO_6 have been known as prospective spintronic materials beyond room temperature[3,5,10,18,20]. On the other hand, double perovskite Sr_2CrOsO_6 is a robust ferrimagnetic insulator with the highest magnetic Curie of 725 K, and its semiconductor gap has been shown to originate from spin-exchange splitting of the Os $5d$ t_{2g} bands[18,21,22]. Very special are double perovskite Ca_2FeReO_6 and Ca_2CrReO_6 whose ground-state phases are ferrimagnetic insulators with monoclinic structure although there are two electrons for their Re $5d$ t_{2g} triplet[14,18]. They have high magnetic Curie temperatures of 522 and 360 K[9,14,18]. Their ferrimagnetic insulating phases have been established experimentally[9,14,18,20,23,35], but their non-metallic electronic properties have not been elucidated yet and their structure-property relationship still needs to be understood, especially in the case of the Ca_2CrReO_6.

Here, we investigate the structural, electronic and magnetic properties of the Ca_2CrReO_6 and Ca_2FeReO_6 through density functional theory calculations in order to reveal the origin of their special electronic structures, especially their semiconductor gaps at low temperature. To accurately calculate the semiconductor gaps, we use Tran and Blahas modified Becke and Johnson (mBJ) approach for the exchange potential[24] to investigate their electronic structures, because its excellent accuracy has been proved for numerous insulators, semiconductors, and transition-metal oxides[24–27]. Our calculations and analyses show that the Ca_2CrReO_6 and Ca_2FeReO_6 still are ferrimagnetic semiconductors even with the spin-orbit effect taken into account, and the semiconductor gaps are formed between the full-filled d_{xy}+d_{xz} doublet and the empty d_{yz} singlet split from the partially-occupied Re 5d t_{2g} triplet around the Fermi level due to the low symmetry in the monoclinic structure. We also explore other properties of the two Ca-based double perovskite compounds in comparison with others similar. More detailed results will be presented in the following.

The rest of the paper is organized as follows. We shall describe our computational details in the next section. In Sec. III we shall present our optimized ground-state structures for the two compounds. In Sec. IV we shall present our spin-dependent density of states, band structures, and electron density distributions and perform further analyses concerned. In Sec. V we shall present our calculated results with the spin-orbit effect taken into account, including their magneto-crystalline anisotropic

energies, spin and orbital moments along the easy axis, and the spin-orbit-effect-modified semiconductor gaps. Finally, we shall give our conclusion in Sec. VI.

II. COMPUTATIONAL DETAILS

We use the full-potential linear augmented plane wave (FP-LAPW) method within the density functional theory (DFT),[28,29] as implemented in the WIEN2k package.[30] We take GGA exchange-correlation functional to do structure optimization and preliminary study[31], and then use mBJ exchange potential to do electronic structure calculations. The scalar relativistic approximation is used for valence states, with the spin-orbit coupling (SOC) is taken into account, whereas the radial Dirac equation is self-consistently solved for the core electrons[32–34]. The magnetization is chosen to be along all nonequivalent directions for the monoclinic structure when we investigate the magneto-crystalline anisotropy. The muffin-tin radii of the Ca, Cr, Fe, Re, and O atoms are set to be 2.20, 1.96, 2.03, 1.96, and 1.71 bohr, respectively. We make harmonic expansion up to $l_{max} = 10$ in the muffin-tin spheres, and set $R_{mt} \times K_{max} = 8.0$. We use 1000 k-points in whole Brillouin zone (234 k-points in the reduced wedge). For testing the accuracy, we also use 2000 k-points to do the self-consistent calculations. The total energy difference is proved to be less than 1 meV. Therefore, our choice of 1000 k-points is enough for the whole calculation. The self-consistent calculations are considered to be converged only when the integration of absolute charge-density difference per formula unit between the successive loops is less than $0.0001|e|$, where e is the electron charge.

III. STRUCTURE OPTIMIZATION

The structure of Ca_2MReO_6 (M=Cr or Fe) has been reported to be monoclinic structure with $P2_1/n$ symmetry (space group #14) at room temperature,[9,18] which is consistent with the prediction of the empirical tolerance factor f.[18,35] The monoclinic structure is fairly distorted from cubic double perovskite due to the small size of Ca^{2+} cation, which forces the MO_6 and ReO_6 octahedra to tilt and rotate in order to optimize the Ca-O bond lengths. The crystal structure for Ca_2MReO_6 (M=Cr or Fe) is demonstrated in Fig. 1. In order to investigate the origin of the nonmetallicity in their ground-state phases, we optimize fully their geometric structures and internal atomic positions by combining total energy and force optimizations. We have considered a larger unit cell of 2 f.u. including 20 atoms to relax the structure. The optimized lattice parameters are listed in Table I, with experimental data included for comparison. The ground state phase is confirmed to be the $P2_1/n$ structure for both of the compounds, with lattice constants expanded slightly with respect to experimental ones. This deviation is due to the special property of the GGA functional. However, the tilt angles β of Ca_2MReO_6 (M=Cr and Fe) decrease by 0.22° and 0.27° with respect to experimental values, respectively, which reflects the large distortion at low temperature.

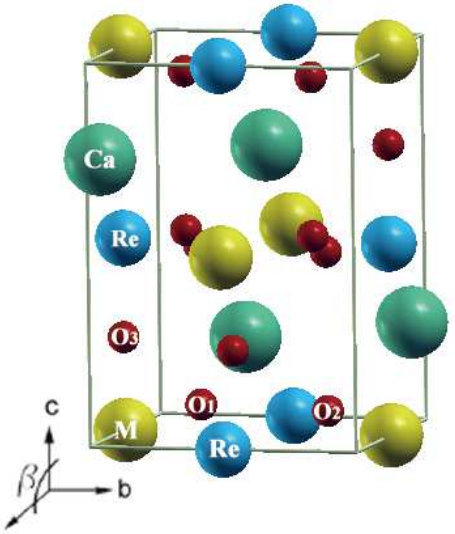

FIG. 1: (color online) The $P2_1/n$ (#14) crystal structure of double perovskites Ca_2MReO_6, with three nonequivalent O atoms labeled. Ca, M, Re, and O atoms are denoted by colored balls with different sizes from the biggest to the smallest, where M denotes Cr or Fe atom. The M and Re atoms form a NaCl-like lattice.

TABLE I: Optimized lattice constants and tilt angle β of Ca_2MReO_6 (M=Cr,Fe) with space group $P2_1/n$ (#14), compared with experimental results[9]

Lattice	Ca_2CrReO_6		Ca_2FeReO_6	
parameters	opt.	exp.	opt.	exp.
a (Å)	5.392	5.388	5.417	5.401
b (Å)	5.524	5.460	5.609	5.525
c (Å)	7.680	7.660	7.733	7.684
β (°)	89.74	89.96	89.80	90.07

We present in Table II optimized bond lengths and bond angles of Ca_2MReO_6 (M=Cr,Fe) with $P2_1/n$ structure. For comparison, we also present the $I4/m$ structure for Ca_2CrReO_6. It's shown that the three Cr-O bond lengths are slightly larger than Re-O ones in Ca_2CrReO_6, while the FeO_6 octahedra are significantly more expanded than ReO_6 octahedra in Ca_2FeReO_6. This observation is consistent with the ionic size sequence of $Re^{5+} < Cr^{3+} < Fe^{3+}$. The bond angles in ReO_6 octahedra all deviate from ideal values of 90°, so do the angles of M-O-Re from 180°. Considering that a large number of double perovskite compounds with half-metallicity are in tetragonal structure with $I4/m$ symmetry (space group #87), and in order to clarify the relationship be-

tween the electronic property and lattice structure, we also present the structure parameters of the $I4/m$ structure for Ca_2CrReO_6 in Table II. There are actually two nonequivalent kinds of O atoms in $I4/m$ structure. The O_1 and O_2 atoms are equal to each other and in the same xy-plane. The atom O_3 sits along the z-axis with Cr or Re atoms in between. The bond lengths of Cr-O are larger than those of Re-O due to the larger ionic size of Cr^{3+} versus Re^{5+}. All angles in ReO_6 octahedra remain to be 90°, while the Cr-$O_{1,2}$-Re bond angles reduce significantly from 180°, which makes the Cr-$O_{1,2}$ and Re-$O_{1,2}$ lengths much larger than the Cr-O_3 and Re-O_3 bonds, respectively. Our calculated total energy of Ca_2CrReO_6 in $I4/m$ structure are higher than that in $P2_1/n$ structure by 392 meV per formula unit, indicating the $P2_1/n$ structure is more stable for Ca_2CrReO_6.

TABLE II: Optimized bond lengths and angles of Ca_2MReO_6 (M=Cr, Fe) with space group $P2_1/n$ (#14), with those of Ca_2CrReO_6 with $I4/m$ (#87) structure for comparison. O_1 and O_2 are equivalent to each other in $I4/m$ structure.

	M	Cr(#14)	Cr(#87)	Fe(#14)
Bond length	M-O_1	1.975	1.984	2.061
	M-O_2	1.978	1.984	2.046
	M-O_3	1.971	1.939	2.036
	Re-O_1	1.974	1.977	1.944
	Re-O_2	1.968	1.977	1.948
	Re-O_3	1.964	1.922	1.941
Bond angle	O_1-Re-O_2	90.88	90	90.30
	O_2-Re-O_3	89.43	90	89.28
	O_1-Re-O_3	89.81	90	89.22
	M-O_1-Re	152.56	154.63	149.34
	M-O_2-Re	152.85	154.63	150.59
	M-O_3-Re	153.46	180	150.06

IV. ELECTRONIC STRUCTURES

A. Density of states and energy bands

From now on, we investigate the electronic structures of the optimized Ca_2MReO_6 (M=Cr,Fe). At first, we use the popular GGA functional to calculate the density of states (DOS). The spin-resolved DOSs are presented in Fig. 2. For the Ca_2CrReO_6, the electronic energy bands between -8.0 eV and -3.0 eV are dominated by O $2p$ states. The Fermi energy falls in an energy gap of about 1.0 eV in the majority spin channel, between the fully filled Cr t_{2g} and empty Re t_{2g} bands. As for the Ca_2FeReO_6, the triplet Fe t_{2g} states in the majority spin channel move to the lower energy between -8.2 eV and -2.2 eV, with a strong mixture of O $2p$ states. The Fermi energy is in the majority-spin gap of 1.4 eV between Fe e_g and Re t_{2g} bands. In contrast, for the minority spin channel, the Fermi level lies in the partially filled t_{2g} bands of hybridized M, Re, and O $2p$ states in the Ca_2MReO_6 (M=Cr,Fe). Thus, the GGA calculation produces a half-metallic ferrimagnet. This is contradictory with the reported experimental results[9,18] and can be attributed to the false GGA description of Re t_{2g} nature around the Fermi level in the monoclinic structure. For the sake of accurate calculation for Re t_{2g} state, we need to use improved exchange potential to investigate electronic structures of the Ca_2MReO_6. The modified Becke-Johnson (mBJ) potential is a good choice because it is excellent in describing the hybrid transition-metal ions.[25,36]

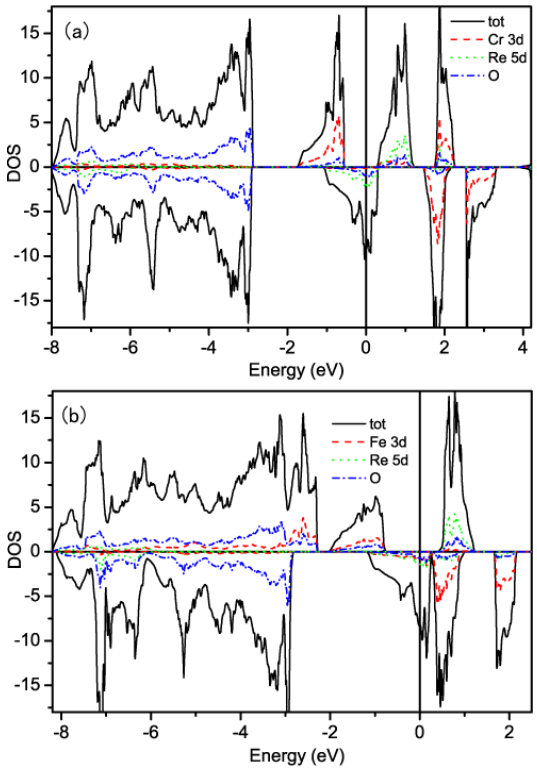

FIG. 2: (color online) The spin-resolved total (tot) and partial (Cr/Fe,Re,O) density of states (DOSs) of Ca_2CrReO_6 (a) and Ca_2FeReO_6 (b) in $P2_1/n$ structure from GGA calculation.

We present the spin-resolved DOSs and energy bands of the Ca_2CrReO_6 calculated with mBJ in Fig. 3. It is clear that there is a semiconductor gap open at the Fermi level, which is in good agrement with experimental results[9]. Moreover, the occupied Cr t_{2g} and unoccupied Cr e_g and Re t_{2g} bands in the majority spin channel are pushed substantially downwards and upwards, respectively, which consequently enhances the majority-spin gap (G_{mag}) to 2.5 eV. In the minority spin channel, the triplet Re t_{2g} states around the Fermi level further split into a doublet d_{xy}+d_{xz} and a singlet d_{yz}, with two electrons fully occupying the doublet state. This produces a semiconductor gap of 0.38 eV, as shown in Fig. 3(a). The detailed orbital-resolved DOSs around the Fermi level are

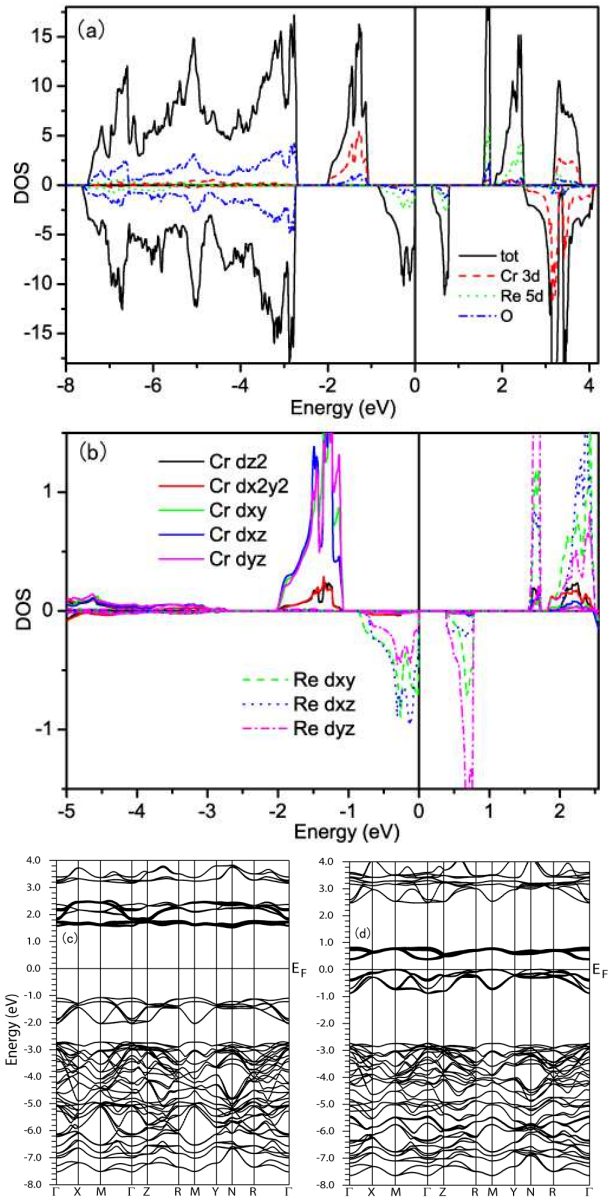

FIG. 3: (color online) Electronic structure of Ca_2CrReO_6 in $P2_1/n$ structure calculated with mBJ: spin-resolved total (tot) and partial (Cr,Re,O) DOSs (a); amplified d states split DOSs of Cr and Re around the Fermi level (b); and majority-spin (c) and minority-spin (d) bands.

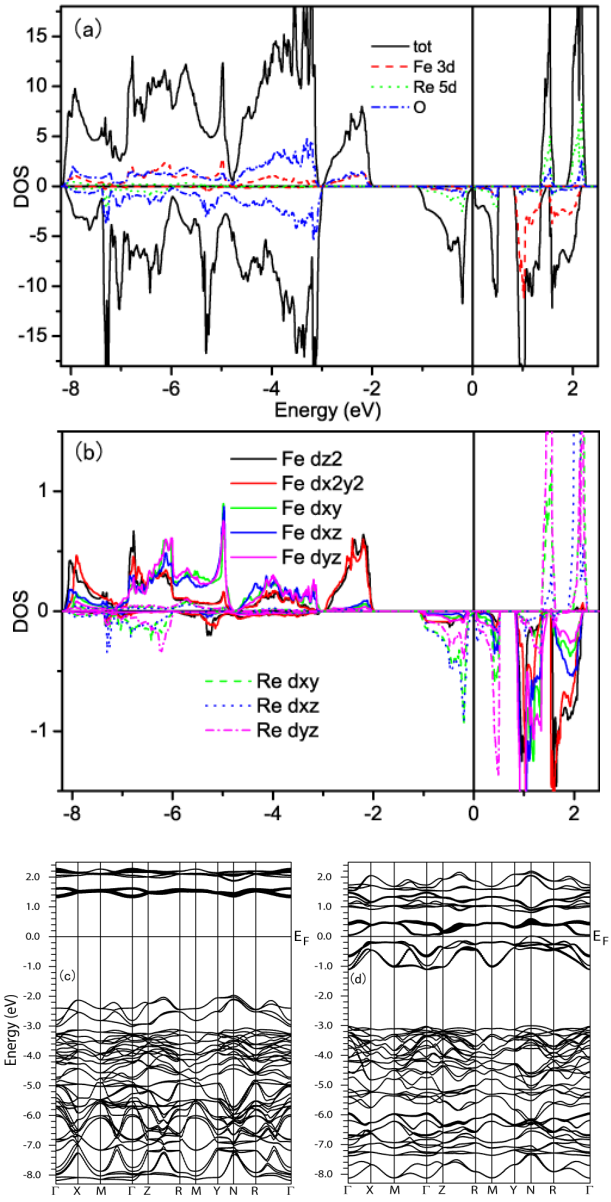

FIG. 4: (color online) Electronic structure of Ca_2FeReO_6 in $P2_1/n$ structure calculated with mBJ: spin-resolved total (tot) and partial (Fe,Re,O) DOSs (a); amplified d states split DOSs of Fe and Re around the Fermi level (b); and majority-spin (c) and minority-spin (d) bands.

presented in Fig. 3(b). Both of the unoccupied Cr t_{2g} and e_g in the minority spin channel are pushed upwards substantially, with a little overlap between them, which enlarges the spin exchange splitting energy of Cr t_{2g} to 4.7 eV. Fig. 3(c) and (d) show the energy bands of the Ca_2CrReO_6 in majority-spin and minority-spin channels, respectively. The thicker a line is, the more the Re t_{2g} weight is. There are 72 bands (36 majority spin and 36 minority spin) in the energy window from -7.8 eV to -2.6 eV, because we consider 2 unit cell in our calculation. The energy bands between -2.0 eV and -1.0 eV consist of 6 Cr t_{2g} bands in the majority spin channel. There are 4 occupied bands of Re t_{2g}, including d_{xy} and d_{xz} just below the Fermi level and 2 bands of d_{yz} above the Fermi level. It can be clearly seen that the top of the valence band and the bottom of the conduction band are located in N and Γ points, respectively, resulting in an indirect band gap for the Ca_2CrReO_6.

In Fig. 4 we present the spin-resolved DOSs and energy bands of the optimized Ca_2FeReO_6 calculated with mBJ. The distinguished feature of the DOSs is that compared to GGA results, the Fe t_{2g} states move to lower energy in the majority spin channel, and the gaps between Fe

t_{2g} and e_g states almost vanish in both of spin channels. This can be attributed to the enhanced spin exchange effect due to mBJ functional. The semiconductor gap of 0.05eV is also observed, owing to the same reason as in the Ca_2CrReO_6. However, the Re t_{2g} splitting in the minority spin channel is much smaller than that in the majority spin channel, in contrast to the Ca_2CrReO_6. This result is consistent with the fact that the resistivity of the Ca_2FeReO_6 at low temperature is almost two order of magnitude lower than that of Ca_2CrReO_6, because the electron inter-band transition takes place easily in the Ca_2FeReO_6 compound. In the band structures (c) and (d) of the Ca_2FeReO_6, the Fe t_{2g} bands are pushed down to between -8.0 eV and -3.0 eV in the majority spin channel, in contrast to the minority-spin one. the energy window from -3.0 eV to -2.0 eV consists of 4 bands of Fe e_g. The energy band distribution around the Fermi level in the minority spin channel is similar to that of the Ca_2CrReO_6. The top of valence bands and the bottom of the conduction bands are located in N and Γ points, respectively. This implies that the semiconductor gap of the Ca_2FeReO_6 is indirect, same as that of the Ca_2CrReO_6.

B. Electron density distributions

The energy-resolved charge and spin density distributions are very important to explore the bonding and magnetic properties. We present in Fig. 5 the valence charge (including up and down) and spin density distributions of the Ca_2CrReO_6, with all the contribution from -8.0 eV to the Fermi level, calculated with mBJ. The upper three panels are for the (001) plane of the structure shown in Fig. 1, the lower three ones are for the perpendicular plane, being equivalent to the (110) plane, including Cr and Re ions. In the spin-up channel, the charge density distributions at Cr sites look like a quatrefoil, which reflects the fully occupied t_{2g} characteristic between -2 eV to -1 eV, whereas the charge density around Re is fairly small. In the spin-down channel, there is much electron density around Re, in consistence with the partially filled Re t_{2g} state from -1 eV to the Fermi level. The small charge density at Cr sits should result from the hybridization between Re and Cr t_{2g} states. In both of the spin channels, the oxygen atoms with high electron affinities attract the electrons from Cr and Re atoms to form nearly closed O $2p$ shells with spherically distributed charge densities. It can be seen in the charge density contours that the bonds between Cr and nearest O are almost ionic with respect to the Re-O bonds with covalent characteristic, which is in accordance with the longer bond lengths of Cr-O than Re-O ones, as described in Table II. The charge distributions also show that there exists no direct interaction between two nearest Cr-Cr or Re-Re pairs. The spin density distribution of the Ca_2CrReO_6 in Fig. 5 (e) and (f) demonstrates that the spin moments of Cr and Re are mainly localized at the ionic sites. The different colors of outermost lines from Cr and Re indicate the antiferromagnetic coupling between the two transition-metal moments in the double perovskite Ca_2CrReO_6. The some deformed quatrefoils of Cr and Re ions are ascribed to the distortion of O octahedra. It is worth notice that different density contours between Re and Cr sites are due to the more closed shells in the inner part of heavier Re ion compared to Cr.

As for the Ca_2FeReO_6, we illustrate the corresponding charge and spin density distributions calculated with mBJ in Fig. 6. It can be seen that charge distributions at the Fe site are nearly spherical because of nearly half-filled Fe $3d$ orbitals, which is different from the quatrefoils shape of partially occupied Cr $3d$ orbitals in the Ca_2CrReO_6. The Fe $3d$ electrons that are more than half full move to oxygen sites for stabilizing the ground state, leaving the highly ionized Fe atoms, as shown in Fig. 6. The shape of charge density around the Re site is similar to that in the Ca_2CrReO_6 due to the same valence states of Re^{5+} ions in the two compounds. Most of the Re $5d$ electrons with larger orbitals spread out to O $2p$ states, forming the Re-O covalent bonds. Furthermore, the hybridizations are still along the Fe-O-Re-O-Fe chain, and no direct interaction between Fe-Fe and Re-Re pairs are found. The spin moments of Fe $3d$ and Re $5d$ states are mainly localized and coupled antiferromagnetically.

C. Further analyses

The spin exchange splitting (Δex) and crystal field splitting (Δcf) of Cr and Fe, the spin exchange splitting Δex of Re ion, and the band gaps across the Fermi level in both majority-spin (G_{maj}) and minority-spin (G_{min}) channels calculated with GGA and mBJ are summarized in Table III. Both Δex and Δcf of transition-metals are significantly enhanced by mBJ calculation. As a result, the gaps in the majority spin channel are enlarged by 1.5 eV and 1.9 eV for the Ca_2MReO_6 (M=Cr,Fe), respectively. The semiconductor gaps are equivalent to 0.38 eV and 0.05 eV, respectively, in contrast to the wrong results from GGA. This implies that the mBJ functional is excellent in describing the hybrid correlated transition-metal ions in Ca_2MReO_6 (M=Cr,Fe) compounds.

TABLE III: Spin exchange splitting (Δex) and crystal field splitting (Δcf) of Cr and Fe, spin exchange splitting Δex of Re ion, the band gaps across the Fermi level in the majority-spin channel (G_{maj}) and the minority-spin channel (G_{min}) of Ca_2MReO_6 (M=Cr, Fe) calculated with GGA and mBJ.

M	scheme	Δex(M)	Δcf(M)	Δex(Re)	G_{maj}	G_{min}
Cr	GGA (eV)	2.9	3.0	0.6	1.0	0
	mBJ (eV)	5.3	4.7	2.0	2.5	0.38
Fe	GGA (eV)	3.0	1.0	0.8	1.4	0
	mBJ (eV)	4.5	1.5	1.8	3.3	0.05

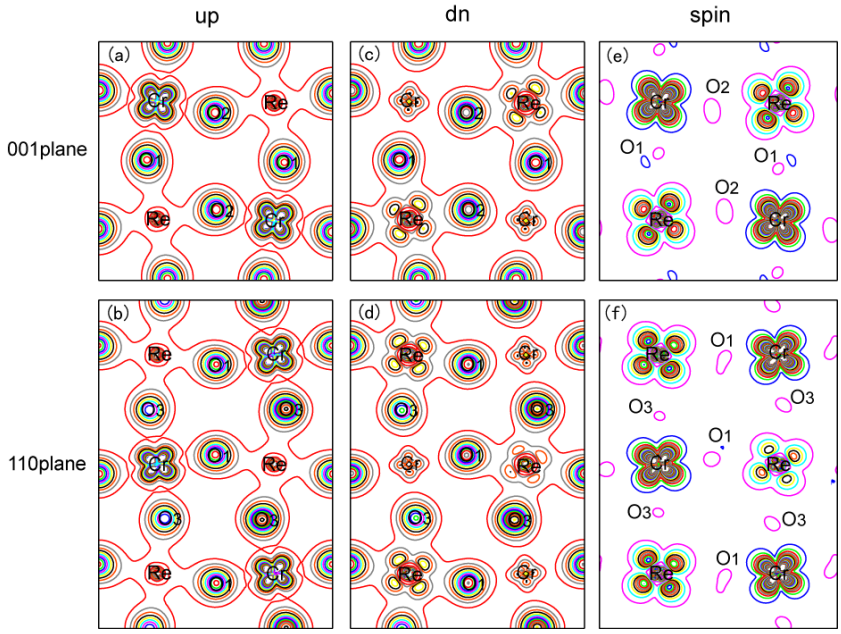

FIG. 5: (color online) Valence electron charge [up, (a) and (b); dn, (c) and (d)] and spin [(e),(f)] density distributions, within the energy window from -8.0 eV to the Fermi level, of Ca_2CrReO_6 projected to the (001) and (110) planes calculated with mBJ. The contours in (a)-(d) are from 0.005 to $0.5e$/a.u.^{3} with an increment of $0.025e$/a.u.^{3}, and those in (e) and (f) from -0.5 to 0 e/a.u.^{3} for Re sites and 0 to $0.5e$/a.u.^{3} for Cr sites with an increment of $0.013e$/a.u.^{3}.

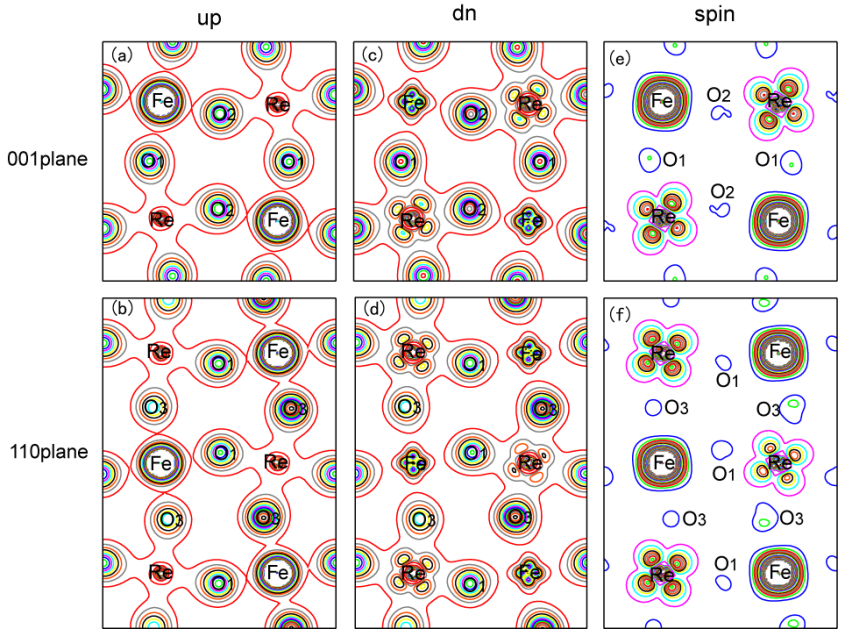

FIG. 6: (color online) Valence electron charge [up, (a) and (b); dn, (c) and (d)] and spin [(e),(f)] density distributions, within the energy window from -8.2 eV to the Fermi level, of Ca_2FeReO_6 projected to the (001) and (110) planes calculated with mBJ. The contours in (a)-(d) are from 0.005 to $0.5e$/a.u.^{3} with an increment of $0.025e$/a.u.^{3}, and those in (e) and (f) from -0.5 to 0 e/a.u.^{3} for Re sites and 0 to $0.5e$/a.u.^{3} for Fe sites with an increment of $0.013e$/a.u.^{3}.

For investigating the intrinsic reason of semiconductor nature in the monoclinic Ca_2MReO_6 (M=Cr,Fe), we calculate the DOSs of the Ca_2CrReO_6 in $I4/m$ structure with both GGA and mBJ functionals. The GGA produces a half-metallicity, which is similar to the GGA result of the Ca_2CrReO_6 with $P2_1/n$ symmetry, and however, the metallic property is not changed by using mBJ potential, although the Δex and Δcf of Cr and Re are much enlarged. This comparison indicates that the semiconductor nature of the Ca_2MReO_6 has intimate relationship with the crystal structure. In $I4/m$ structure, the bond angles of ReO_6 octahedra are ideal 90°. The Re $5d$ states are divided into triply degenerate t_{2g} states and doubly degenerate e_g states. Thus, the Fermi level across the partially filled Re t_{2g} in the minority-spin channel. As for $P2_1/n$ structure, the ReO_6 octahedra undergoes tilting and rotation, making the bond angles all deviate from 90°, as listed in Table II. Therefore, the triplet Re t_{2g} states are further split into a doublet d_{xy}+d_{xz} and a singlet d_{yz} due to the Jahn-Teller distortion, producing a crystalline field splitting band gap, in contrast to the former Mott-Hubbard gap.[9,20,23] This fact is consistent with the quatrefoil pattern of the spin density distribution at Re sites, as shown in Fig. 5(e) and (f) and Fig. 6 (e) and (f). The larger gap obtained in the Ca_2CrReO_6 compound can be attributed to the stronger distortion of ReO_6 octahedron than in the Ca_2FeReO_6.

V. SPIN-ORBIT COUPLING EFFECT

To investigate the effect of spin-orbit coupling on the optimized Ca_2MReO_6 (M=Cr,Fe), the magnetization is chosen to be approximately along [100], [010], [001], [110], [101], [011] and [111] directions for the $P2_1/n$ monoclinic structure. The calculated total energies with GGA+SOC method presented in Table IV indicate high magneto-crystalline anisotropy (MAC) in the Ca_2MReO_6 compounds. The most stable magnetic orientation are both along [010] direction, equivalent to the b-axis perpendicular to the ac plane in the $P2_1/n$ structure. These are consistent with experimental results[18].

TABLE IV: Total energies (meV) of Ca_2MReO_6 (M=Cr,Fe) with different magnetization orientations calculated with GGA+SOC, with the lowest energy set as reference.

M	[100]	[010]	[001]	[110]	[101]	[011]	[111]
Cr	1.00	0	2.16	1.21	2.08	1.34	1.29
Fe	1.37	0	2.04	2.03	2.62	1.60	1.61

TABLE V: The mBJ results of individual and total spin moments (μ^s), orbital moments (μ^o), and net moments ($\mu_{\rm tot}$) in μ_B, and semiconductor gap (G_s, in eV) of Ca_2MReO_6 (M=Cr,Fe) with $P2_1/n$ structure with and without SOC.

M	scheme	μ^s_M	$\mu^s_{\rm Re}$	$\mu^s_{\rm tot}$	μ^o_M	$\mu^o_{\rm Re}$	$\mu_{\rm tot}$	G_s
Cr	mBJ	2.520	-1.264	1.000			1.000	0.38
	mBJ+SOC	2.520	-1.239	1.035	-0.018	0.192	1.209	0.31
Fe	mBJ	4.090	-1.118	3.000			3.000	0.05
	mBJ+SOC	4.090	-1.096	3.033	0.042	0.183	3.258	0.03

After the magnetic easy axis is fixed, we do further study with SOC along the [010] direction. Our calculated spin and orbital moments for the Ca_2MReO_6 are summarized in Table V. When SOC is neglected, the total spin moment is precisely $1\mu_B$ and $3\mu_B$ per formula unit for the Ca_2CrReO_6 and Ca_2FeReO_6, respectively. The results can be elucidated in the ionic model, where the transition-metal ions are in the $(M{\rm Re})^{8+}$ valence state. The M^{3+} are in the high spin state of S=3/2 for Cr^{3+} and S=5/2 for Fe^{3+} according to Hund's rule, antiferromagnetically coupled with highly ionized Re^{5+} with valence spin states of S=1, resulting the integer moment in Bohr magneton. Note that a large part of the spin moment is delocalized into the interstitial region, and therefore the spin moments of the individual M and Re ions appear small compared to the ionic values.

When SOC is taken into account, the total spin moments increase by $0.035\mu_B$ and $0.033\mu_B$ for the Ca_2MReO_6 (M=Cr,Fe), respectively, due to some increase of Re spin moment. The orbital moments of Cr and Re are both antiparallel to the spin moments, because of the less than half-filled d shell, in accordance with Hund's rule. As for the Ca_2FeReO_6, the orbital moments of Fe $3d$ is of the same sign as the spin moment, indicating that the $3d$ orbital is more than half-filled, consistent with Hund's rule. Our calculated Cr orbital moment of -0.018μ_B is much smaller than the Cr one of $0.042\mu_B$, which could be understood as a consequence of stronger ligand field caused by the Cr $3d$ orbital than by the Fe $3d$ orbital. For Re ion, the orbital moment is $0.192\mu_B$ or $0.183\mu_B$ for the Ca_2CrReO_6 or Ca_2FeReO_6, due to the strong spin-orbit coupling in $5d$ orbital. The higher improvement of total magnetic moment, $0.258\mu_B$, in the Ca_2FeReO_6 than $0.209\mu_B$ in the Ca_2CrReO_6 is due to the positive large orbital moment in Fe ion.

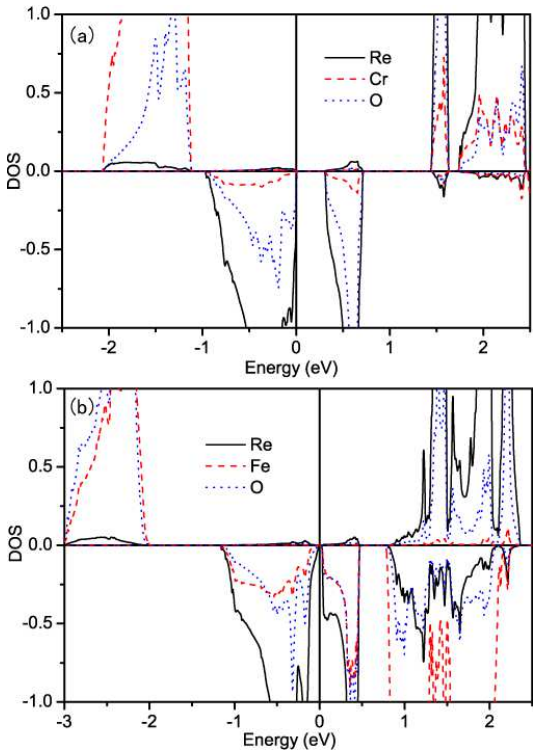

FIG. 7: (color online) The spin-resolved DOS of Ca_2CrReO_6 (a) and Ca_2FeReO_6 (b) calculated with mBJ potential and SOC taken into account.

We also present the semiconductor gaps G_s as the true gaps of these compounds in Table V. When SOC is included, the band gaps remain but become smaller, and is equivalent to 0.31 eV for the Ca_2CrReO_6 and 0.03 eV for the Ca_2FeReO_6, respectively. In order to understand in more detail the reason of the smaller gap with SOC, the partial DOS of M and Re projected onto d orbital in the Ca_2MReO_6 calculated with SOC are plotted in Fig. 7. In the presence of SOC, the bands in both of the spin channels hybridize with each other, in contrast to the pictures in Figs. 3 and 4. The Re t_{2g} states around the Fermi level in one spin channel induce some states in the oppositive spin channel, especially in the Ca_2FeReO_6 compound. Moreover, the Re t_{2g} characteristic states with SOC are broadened compared with those without

SOC, which leads to the some reduction of the semiconductor gaps of the Ca_2MReO_6. It should be pointed out that the noninteger moments in Bohr magneton in the Ca_2MReO_6 (M=Cr,Fe) with $P2_1/n$ structure are the consequence of the mixing of spin-up and spin-down states, but the semiconductor gaps are preserved.

VI. CONCLUSION

We have used FP-LAPW method to investigate the structural, electronic, and magnetic properties of double perovskites Ca_2MReO_6 (M=Cr,Fe). The GGA approach has been used to do geometry optimization, and then the electronic and magnetic properties have been investigated with mBJ exchange potential for improving on calculational accuracy. Our calculated results confirm the ground-state $P2_1/n$ structure for both of the Ca_2MReO_6. The mBJ calculation reveals the semiconductor characteristic with gaps of 0.38 eV and 0.05 eV, respectively, being consistent with the experimental results at low temperature[9,14,18,20,23,35]. The correct mBJ result of the electronic states is because the mBJ potential improves on the DFT description of both crystal field and spin exchange splitting in such compounds.

The origin of semiconductor state of the double perovskite Ca_2MReO_6 is due to the crystalline distortion of ReO_6 octahedra in the $P2_1/n$ structure, which drives the further splitting of partially-occupied Re^{5+} t_{2g} state into a full-filled doublet d_{xy}+d_{xz} and an empty singlet d_{yz} in the minority-spin channel. Thus, The semiconductor gap is formed from the crystalline field splitting in one single spin channel, in contrast to the pervious proposed Mott-Hubbard insulator state. The total spin moments of the Ca_2MReO_6 (M=Cr,Fe) in the semiconductor ground-states are found to be $1\mu_B$ and $3\mu_B$ per formula unit without the spin-orbit effect included, respectively. When the spin-orbit coupling is taken into account, the total magnetic moments become noninteger in unit of Bohr magneton as consequence of the mixing of spin-up and spin-down states. Fortunately, the semiconductor gaps (0.31 and 0.03 eV) remain open and robust in this structure even when SOC effect is included.

In summary, our DFT investigation with mBJ has established the correct ferrimagnetic semiconductor ground state for the double perovskites Ca_2MReO_6 (M=Cr,Fe), which originate mainly from the crystalline field splitting of the three partially-occupied Re t_{2g} bands into two full-filled doublet bands and one empty singlet band near the Fermi level. This mechanism is different from that in Sr_2CrOsO_6, and can help understand physical properties of other similar compounds.

Acknowledgments

This work is supported by Nature Science Foundation of China (Grant No. 11174359), by Chinese Department of Science and Technology (Grant No. 2012CB932302), and by the Strategic Priority Research Program of the Chinese Academy of Sciences (Grant No. XDB07000000).

* Corresponding author: bgliu@iphy.ac.cn

[1] S. A. Wolf, D. D. Awschalom, R. A. Buhrman, J. M. Daughton, S. von Molnár, M. L. Roukes, A. Y. Chtchelkanova, and D. M. Treger, Science **294**, 1488 (2001).
[2] M. T. Anderson, K. B. Greenwood, G. A. Taylor, and K. R. Poeppelmeier, Prog. Solid State Chem. **22**, 197 (1993).
[3] K. I. Kobayashi, T. Kimura, H. Sawada, K. Terakura, and Y. Tokura, Nature (London) **395**, 677 (1998).
[4] W. E. Pickett, Phys. Rev. B **57**, 10613 (1998).
[5] K. I. Kobayashi, T. Kimura, Y. Tomioka, H. Sawada, K. Terakura, and Y. Tokura, Phys. Rev. B **59**, 11159 (1999).
[6] A. Arulraj, K. Ramesha, J. Gopalakrishnan, and C. N. R. Rao, J. Solid State Chem. **155**, 233 (2000).
[7] Y. Moritomo, S. Xu, A. Machida, T. Akimoto, E. Nishibori, M. Takata, and M. Sakata, Phys. Rev. B **61**, R7827 (2000).
[8] M. G. Hernández, J. L. Martinez, and J. A. Alonso, Phys. Rev. Lett. **86**, 2443 (2001).
[9] H. Kato, T. Okuda, Y. Okimoto, Y. Tomioka, K. Oikawa, T. Kamiyama, and Y. Tokura, Phys. Rev. B **69** 184412 (2004).
[10] G. Vaitheeswaran, V. Kanchana, and A. Delin, Appl. Phys. Lett. **86**, 032513 (2005).
[11] N. S. Rogado, J. Li, A. W. Sleight, and M. A. Subramanian, Adv. Mater. **17**, 2225 (2005).
[12] A. J. Hauser, R. E. A. Williams, and F. Yang, Phys. Rev. B **83**, 014407 (2011).
[13] H. P. Wu, Y. Qian, and R. F. Lu, Appl. Phys. Lett. **99**, 123116 (2011).
[14] A. Winkler, N. Narayanan, D. Mikhailova, K. G. Bramnik, H. Ehrenberg, H. Fuess, G. Vaitheeswaran, V. Kanchana, F. Wilhelm, A. Rogalev, A. Kolchinskaya, and L. Alff, New J. Phys. **11**, 073047 (2009).
[15] O. Erten, O. N. Meetei, A. Mukherjee, M. Randeria, N. Trivedi, and P. Woodward, Phys. Rew. Lett. **107**, 257201 (2011).
[16] A. F. Garcia-Flores, A. F. L. Moreira, U. F. Kaneko, F. M. Ardito, H. Terashita, M. T. D. Orlando, J. Gopalakrishnan, K. Ramesha, and E. Granado, Phys. Rew. Lett. **108**, 177202 (2012).
[17] C. Du, R. Adur, H. Wang, A. J. Hauser, F. Yang, and P. C. Hammel, Phys. Rew. Lett. **110**, 147204 (2013).
[18] D. Serrate, J. M. De Teresa, and M. R. Ibarra, J. Phys.: Condens. Matter **19**, 023201 (2007).
[19] T. K. Mandal, C. Felser, M. Greenblatt, and J. Kübler, Phys. Rev. B **78**, 134431 (2008)
[20] H. Kato, T. Okuda, Y. Okimoto, Y. Tomioka, Y. Takenoya, A. Ohkubo, M. Kawasaki, and Y. Tokura, Appl. Phys. Lett. **81**, 328 (2002).
[21] Y. Kronkenberger, K. Mogare, M. Reehuis, M. Tovar, M.

Jansen, G. Vaitheeswaran, V. Kanchana, F. Bultmark, A. Delin, F. Wilhelm, A. Winkler, and L. Alff, Phys. Rev. B **75**, 020404(R) (2007).

[22] O. N. Meetei, O. Erten, M. Randeria, N. Trivedi, and P. Woodward, Phys. Rev. Lett. **110**, 087203 (2013).

[23] H. Kato, T. Okuda, Y. Okimoto, Y. Tomioka, K. Oikawa, T. Kamiyama, and Y. Tokura, Phys. Rev. B **65**, 144404 (2002).

[24] F. Tran and P. Blaha, Phys. Rev. Lett. **102**, 226401 (2009).

[25] D. J. Singh, Phys. Rev. B **82**, 155145 (2010); **82**, 205102 (2010).

[26] S. Gong and B. G. Liu, Phys. Lett. A **375**, 1477 (2011); Chin. Phys. B **21**, 057104 (2012).

[27] S. D. Guo and B. G. Liu, Chin. Phys. B **21**, 017101 (2012).

[28] P. Hohenberg and W. Kohn, Phys. Rev. **136**, B864 (1964).

[29] W. Kohn and L. J. Sham, Phys. Rev. **140**, A1133 (1965).

[30] P. Blaha, K. Schwarz, G. K. H. Madsen, D. Kvasnicka, and J. Luitz, *WIEN2k an Augmented Plane Wave + Local Orbitals Program for Calculating Crystal Properties* (Karlheinz Schwarz Technische Universität Wien, Austria, 2001).

[31] J. P. Perdew, K. Burke, and M. Ernzerhof, Phys. Rev. Lett. **77** 3865 (1996).

[32] A. H. MacDonald, W. E. Pickett, and D. D. Koelling, J. Phys. C: Solid State Phys. **13**, 2675 (1980).

[33] J. Kunes, P. Novak, R. Schmid, P. Blaha, and K. Schwarz, Phys. Rev. B **64**, 153102 (2001).

[34] D. D. Koelling and B. N. Harmon, J. Phys. C: Solid State Phys. **10** 3107 (1977).

[35] J. Gopalakrishnan, A. Chattopadhyay, S. B. Ogale, T. Venkatesan, R. L. Greene, A. J. Millis, K. Ramesha, B. Hannoyer, and G. Marest, Phys. Rev. B **62**, 9538 (2000).

[36] D. Koller, F. Tran, and P. Blaha, Phys. Rev. B **83**, 195134 (2011).